https://doi.org/10.5194/acp-2020-787
Preprint. Discussion started: 24 September 2020

Atmospheric Chemistry and Physics Discussions

Characteristics of the summer atmospheric boundary layer height over the Tibetan Plateau and influential factors

Junhui Che[1, 2, 3], Ping Zhao[1]

[1]State Key Laboratory of Severe Weather, Chinese Academy of Meteorological Sciences, Beijing, 100081, China
[2]College of Atmospheric Science, Nanjing University of Information Science and Technology, Nanjing, 210044, China
[3]Shandong Meteorological Service Center, Jinan, 250031, China

Correspondence to: Ping Zhao (zhaop@cma.gov.cn)

Abstract. Based on intensive sounding, surface sensible heat flux, solar radiation, and soil moisture observational datasets from the Third Tibetan Plateau Atmospheric Scientific Experiment and the routine meteorological operational sounding and total cloudiness datasets in the Tibetan Plateau (TP) for the period 2013-2015, we investigate the features of summer atmospheric boundary layer (ABL) over the TP and its major influential factors. It is found that the convective boundary layer (CBL) and the neutral boundary layer (NBL) show remarkable diurnal variations over the TP, while the stable boundary layer (SBL) diurnal variation is weak. In the early morning, the ABL height distribution is narrow, with a small west-east difference. The SBL accounts for 85% of the TP ABL. At noon, there is a wide distribution in the ABL height up to 4000 m. The CBL accounts for 77% of the TP ABL, with more than 50% of the CBL height above 1900 m. The ABL height exhibits a large west-east difference, with a mean height above 2000 m in the western TP and around 1500 m in the eastern TP. In the late afternoon, the CBL and SBL dominate the western and eastern TP, respectively, resulting in a larger west-east difference of 1054.2 m between the western and eastern TP. The high ABL height in a cold environment over the western TP (relative to the plain areas) is similar to that in some extreme hot and arid areas such as Dunhuang and Taklimakan Deserts. For the western (eastern) TP, there is low (high) total cloud coverage, with large (small) solar radiation at the surface and dry (wet) soil. These features result in high (low) sensible heat flux and thus promotes (inhibits) the local ABL development.

1 Introduction

The Atmospheric boundary layer (ABL) commonly refers to the bottom layer of the troposphere that is directly affected by the underlying surface conditions with a response time scale of one hour or less (Stull, 1998). The ABL, as the interface for the exchanges of water vapour, momentum, heat, and matter between the surface and the free atmosphere, plays important roles in weather, climate, and the transport of air pollution (Stull, 1988; Garratt, 1992; Huang et al., 2007; Miao et al., 2015). The ABL height is a key variable for diagnosing turbulent mixing, vertical disturbance, convective transmission, atmospheric pollutant dispersion, and atmospheric environmental capacity (Seibert et al., 2000; Guo et al., 2009; Dai et al.,

https://doi.org/10.5194/acp-2020-787
Preprint. Discussion started: 24 September 2020


Atmospheric Chemistry and Physics Discussions

2014; Pal et al., 2015). Therefore, the accurate specification of the ABL height is essential to develop weather, climate, and air pollution prediction models.

The ABL can generally be divided into three types, that is, the convective boundary layer (CBL), the stable boundary layer (SBL), and the neutral boundary layer (NBL) (Stull, 1998). During the daytime, when sufficient solar radiation reaches the surface, the CBL usually dominates (Chen et al., 1997), with unstable thermal stratification and vigorous turbulence. At night, infrared cooling at the surface results in the nocturnal SBL (Zhang et al., 2011a; Miao et al., 2015), with ground-based temperature inversion and weak turbulent motion. The NBL occurs mainly in high wind conditions, particularly combining with thick and extended cloud coverage, and also occurs during the sunrise and sunset transition periods, with turbulence of almost the same intensity in all directions (Blay-Carreras et al., 2014).

The ABL height can be calculated from temperature, humidity, and wind profiles (Seibert et al., 2000; Seidel et al., 2010; Davy, 2018). The CBL height is generally less than 2000–3000 m and the SBL thickness is not more than 400–500 m (Garratt, 1992). The ABL height shows an obvious spatial variation due to differences in topography, thermal properties of the underlying surface, and weather conditions. For example, the CBL can grow to as high as 4700 m in New Delhi before the outbreak of the South Asian monsoon, whereas it may only reach 900 m in Bangalore during the monsoon period (Raman et al., 1990). Seidel et al. (2012) pointed out that a large east-west spatial gradient of the ABL height at sunset in the United States may be related to a difference in the solar altitude angle with respect to latitude. Guo et al. (2016) identified three large-scale spatial patterns in the ABL height in China, that is, a west-east gradient during sunrise, an east-west gradient during sunset, and a south-north gradient at noon. The reasons for the first two patterns are similar to those observed in the United States shown in Seidel et al. (2012), while the south-north gradient may be related to local surface and hydrological processes (Guo et al., 2016; Zhang et al., 2017).

The Tibetan Plateau (TP) with an average elevation exceeding 4500 m has complex land surface processes and boundary layer structures (Tao and Ding, 1981; Yanai and Li, 1994; Xu et al., 2002; Yang et al., 2004; Li et al., 2007; Sun et al., 2007; Zhao et al., 2018). The ABL height is generally higher compared to some plains areas (with the ABL height of 1000–1500 m) (Zhao et al., 1992). Some studies have addressed that the ABL height in the TP can be as high as 2000–3000 m (Ye et al., 1979; Xu et al., 2002; Zhang et al., 2003). Song et al. (1984) examined the ABL height at Gaize station of the western TP is above 3000 m, while the ABL heights obtained by Li et al. (2000), Liu et al. (2001), and L ü et al. (2008) are lower in the central TP (between 400 m and 1800 m at Dangxiong station and 1750 m at Namucuo Lake). Moreover, there is a significant difference in the ABL height over the TP between dry and rainy seasons (Zuo et al., 2004). Li et al. (2011) found that the ABL height at Naqu station is 2211–4430 m in the dry season and 1006–2212 m in the rainy season. Chen et al. (2013, 2016) observed the super-thick ABL at Gaize station during winter, with the ABL height above 5000 m. These results show that the ABL height over the TP varies greatly with position and season.

https://doi.org/10.5194/acp-2020-787
Preprint. Discussion started: 24 September 2020


Atmospheric Chemistry and Physics Discussions

Although observations in the TP and studies on the local ABL features have made progress, routine meteorological operational sounding observations are scarce over the western TP, owing to its high elevations, naturally harsh environmental conditions, and less-developed logistics. The previous studies on the ABL over the western TP are often based on a short-time experimental observational data at Gaize in one summer (Song et al., 1984; Chen et al., 2013). Thus the interpretation of their results has certain limitations. Moreover, there are significant differences in surface properties and climatic conditions between the eastern and western TP (Wang et al., 2016). However, few studies have examined this west-east difference in ABL due to the scarce data in the western TP. To obtain a longer observational data in the western TP, the Third Tibetan Plateau Atmospheric Scientific Experiment (TIPEX-III) beginning in 2013 has deployed routine sounding systems at Shiquanhe, Gaize, and Shenzha stations of the western TP (Fig. 1), which fills in the data gaps in the operational sounding network over the western TP (Zhao et al., 2018). Compared to the previous field experiments over the TP, the TIPEX-III has a wider and longer coverage of sounding observations over the western TP, providing valuable observational data for studying the ABL features.

This study utilizes the TIPEX-III sounding observational data to investigate the features of the ABL height over the TP, compares differences in the ABL height between the western and eastern parts of the TP, and analyzes the major factors affecting the ABL height. The remainder of this paper is organized as follows. Main features of data and methods are described in Section 2. In Section 3, the characteristics of the ABL height over the eastern and western TP and their regional differences are analyzed in detail. Section 4 gives major factors affecting the ABL height over the TP and the west-east differences. Discussions and conclusions are given in Section 5.

2 Data and analysis methods

The TIPEX-III carried out the intensive routine meteorological sounding observations at Shiquanhe (SQH), Gaize (GZ), and Shenza (SZ) stations of the western TP (marked by red dots in Fig. 1) since the 2013 summer (Zhao et al., 2018). These intensive observations have been applied in research on the vertical structure of the upper troposphere and lower stratosphere at Gaize station during the rainy season and effects of assimilating the intensive sounding data on downstream rainfall (Hong et al., 2016; Yu et al., 2018; Zhao et al., 2018; Zhao et al., 2019b). These intensive sounding data and the routine meteorological operational sounding data at 16 stations of the central-eastern TP from the China Meteorological Administration (marked by black dots in Fig. 1) are utilized in this study. The sounding observations were carried out at 08:00 Beijing Time (BJT; 00:00 UTC), 14:00 BJT (06:00 UTC), and 20:00 BJT (12:00 UTC) each day for the above intensive and operational sounding stations, including vertical profiles of temperature, humidity, and wind direction and speed. After the quality of the sounding observational data, we finally select the periods from 15 June to 31 July 2013, from 15 June to 31 August 2014, and from 1 June to 31 August 2015 in this study. There are a total of 11,635 sounding profiles

https://doi.org/10.5194/acp-2020-787
Preprint. Discussion started: 24 September 2020


Atmospheric Chemistry and Physics Discussions

(Fig. 1a) and 4757, 2049, and 4841 profiles separately at 08:00 BJT (Fig. 1b), 14:00 BJT (Fig. 1c), and 20:00 BJT (Fig. 1d) for 19 stations over the TP. Meanwhile, it is noted that there is a large difference in the sample number between the intensive and operational observation records at 08:00 BJT and 20:00 BJT (Fig. 1b and d), which is called the original dataset for convenience. Thus we also select the operational observation records that correspond to the intensive observation records (called the test group dataset for convenience) at these two times and repeat the related analyses, obtaining the similar results (shown in Section 3.2), which shows that the difference in the sample number between the intensive and operational observation records does not change our conclusions.

To analyze the factors affecting the ABL in the TP, we use the TIPEX-III 30-min mean surface sensible heat flux (SHF), downward solar radiation, and 5-cm soil volume moisture content at SQH (bare soil with few obstacles), Naqu (NQ; alpine steppe), and Linzhi (LZ; alpine meadow with few shrubs and trees) stations in the 2014-2015 summers (Wang et al., 2016; Zhao et al., 2018; Li et al., 2019, 2020). In addition, the operational observation of total cloudiness (cloud cover) at 02:00 BJT, 08:00 BJT, 14:00 BJT, and 20:00 BJT from the China Meteorological Administration are also used.

We use the potential temperature gradient method proposed by Liu et al. (2010) to calculate the ABL height. Following Liu et al. (2010), Zhang et al. (2017), and Zhao et al. (2019a), the original sounding observation data are interpolated to new profiles with a vertical resolution of 5 hPa (corresponding to a vertical interval of about 50 m in the ABL) for the ABL classification and height calculation. On the basis of a potential temperature difference (*PTD*) between the fifth layer (~250 m; θ_5) and the second layer (~50 m; θ_2), the ABL is classified as follows.

$$PTD = \theta_5 - \theta_2 \begin{cases} < -\sigma, & \text{for CBL} \\ > +\sigma, & \text{for SBL.} \\ else, & \text{for NBL} \end{cases}$$

Here σ is a critical value. Consistent with Liu et al. (2010) and Zhang et al. (2017), σ is set to 1.0 K. The ABL height is also calculated on the basis of their methods. For both the CBL and NBL, the ABL height is calculated as the height at which an air parcel rising adiabatically from the surface becomes neutrally buoyant (Stull 1988). The SBL height is defined as the lower of the heights of both the thermal stable layer from the surface and the maximum wind shear in the low-level jet stream.

3 Characteristics of the ABL height over the eastern and western TP

3.1 A general characteristic of the ABL height

Diurnal variation is an important feature of the ABL, which consists of different periods of daytime, nighttime, and diurnal transitions (from day to night and from night to day) (Liu et al., 2010). In the central TP (near 90 °E), 08:00 BJT, 14:00 BJT, and 20:00 BJT correspond to 06:00 (the early morning), 12:00 (noon), and 18:00 (the late afternoon) local standard time,

https://doi.org/10.5194/acp-2020-787
Preprint. Discussion started: 24 September 2020


Atmospheric Chemistry and Physics Discussions

respectively. To reveal a difference in the ABL height between the eastern TP (ETP) and the western TP (WTP), we divide all sounding stations over the TP into two groups. One is for the WTP (to the west of 92.5 °E) with 8 stations, and the other is for the ETP (to the east of this longitude) with 11 stations.

Figure 2a-c shows the horizontal distribution of the mean ABL height over the TP at 08:00 BJT, 14:00 BJT, and 20:00 BJT, respectively. In the early morning (08:00 BJT) (Fig. 2a), the ABL height is generally low (<450 m) over the TP and shows a relatively homogeneous feature. At this moment, the distribution of the ABL height is narrow, with a frequency peak of 35% at the ABL height of 300 m (Fig. 2d) and 78.5% (99.6%) of the ABL height below 500 m (1000 m) (Fig. 2e). Figure 2f displays the zonal sections of the ABL height along 32 °N. In this figure, the ABL height varies between 218.4 m and 433.9 m from east to west, not showing a remarkable west-east difference.

At noon (14:00 BJT) (Fig. 2b), the ABL height remarkably increases over the TP, with an average of 1887.7 m, and exhibits a large west-east difference. There is a wide distribution of the ABL height up to 4000 m, with a relatively flat peak between 900 m and 2900 m (Fig. 2d) and only 17.8% (more than 50%) of the ABL height below 1000 m (above 1900 m) (Fig. 2e). The regional mean ABL height is 2124.2 m in the WTP and 1693.5 m in the ETP, with a mean difference of 430.7 m between the WTP and the ETP. Along 32 °N, the ABL height remarkably increases from 1379.4 m at GanZ station to 2504.2 m at SQH station, with the west-east difference exceeding 1200 m (Fig. 2f).

In the late afternoon (20:00 BJT) (Fig. 2c), the ABL height continues to increase in the WTP, with the regional mean height > 2000 m, while it begins to decrease in the ETP, with the regional mean height < 1000 m. This result indicates a larger west-east difference of 1054.2 m between the WTP and the ETP. Especially, the ABL height is 602 m at HY station and 2920.6 m at SQH, with a difference above 2000 m between these two stations (Fig. 2f). At this moment, the frequency of the high ABL height decreases. The frequency peak is 12.8% at the ABL height of 300 m (Fig. 2d) and 50% of the ABL heights are less than 1000 m (Fig. 2e). It is evident that in daytime the ABL height exhibits an increasing trend from east to west in the TP. This west-east difference increases from noon to the late afternoon. The ABL height reaches the maximum in the late afternoon.

3.2 Characteristics of SBL, NBL, and CBL heights

We further examine the characteristics of different ABL types. Figure 3a-c shows the spatial distribution of the SBL height at 00:80 BJT, 14:00 BJT, and 20:00 BJT. It is obvious that the SBL height is generally low and varies between 200 m and 730 m, with a mean height of 336.0 m at 08:00 BJT, 356.0 m at 14:00 BJT, and 321.9 m at 20:00 BJT, not showing a remarkable diurnal variation. For the NBL and CBL, their boundary layer heights are still low in the early morning (Fig. 3d and 3g), with the ABL height < 450 m. In daytime, the NBL and CBL heights remarkably increase, especially in the WTP, with an increasing trend from east to west. At 14:00 BJT (Fig. 3e and 3h), there is a regional mean NBL/CBL height of

https://doi.org/10.5194/acp-2020-787
Preprint. Discussion started: 24 September 2020


Atmospheric Chemistry and Physics Discussions

2074.6 m/2191.4 m in the WTP and 1594.8 m/1788.0 m in the ETP, with a difference of 479.8 m/403.4 m between the WTP and the ETP. At 20:00 BJT (Fig. 3f and 3i), the NBL/CBL height continues to increase in the WTP, with a regional mean of 2092.0 m/2192.2 m, while the NBL/CBL height decreases in the ETP, with a regional mean of 1423.1 m/1237.2 m. For the NBL and CBL, there are larger differences of 668.9 m and 955.0 m in the ABL height between the WTP and ETP, respectively.

Figure 4 shows the distribution of occurrence frequency of different ABL types at 08:00 BJT, 14:00 BJT, and 20:00 BJT. It is clear that the occurrence frequency shows significant diurnal variations for the SBL and CBL. At 08:00 BJT, the occurrence frequency of the SBL/CBL is large/little (Fig. 4a/Fig. 4g), with a mean value 84.9%/8.5% over the TP. At 14:00 BJT, the occurrence of the SBL/CBL remarkably decreases/increases, accounting for 3.1%/76.9% of the ABL (Fig. 4b/Fig. 4h). At 20:00 BJT, the SBL/CBL mainly occurs in the ETP/WTP (Fig. 4c/Fig. 4i), with a regional mean of 35.0%/65.0%. This feature is likely related to a difference in the solar elevation angle with respect to longitude because night begins earlier in the WTP than in the ETP, which supports an earlier transition from the daytime CBL to the nighttime SBL in the east (Seidel et al., 2012; Guo et al., 2016). However, the NBL shows a relatively weaker diurnal variation over the TP (Fig. 4d-f), with the mean occurrence frequency of 6.4%, 20.0%, and 25.5% at 08:00 BJT, 14:00 BJT, and 20:00 BJT, respectively.

Figure 5 shows the ABL height-occurrence frequency relationship for the SBL, NBL, and CBL at 08:00 BJT, 14:00 BJT, and 20:00 BJT. For the SBL, the frequency distribution of the ABL height shows the similar feature at three measurement times (Fig. 5a-c) and is characterized by a narrow single mode, with the frequency peaks of 39.0%, 28.1%, and 36.6% at the boundary layer height of 200 m, 300 m, and 300 m at 08:00 BJT, 14:00 BJT, and 20:00 BJT, respectively. It is found that the SBL height above 80% is < 600 m and the cumulative frequency of the SBL height exceeding 1000 m is little (near zero) at these three times (Fig. 5d, e, and f). The ABL heights of the NBL and CBL show large variations. At 08:00 BJT (Fig. 5a), the distributions of the NBL and CBL height are narrow, with the frequency peaks of 27.5% and 35.1% at the ABL height of 300 m for NBL and CBL, respectively, similar to that of the SBL, which is possibly due to the initial development of the CBL and NBL. At 14:00 BJT (Fig. 5b), there is a wide distribution of the ABL height up to 4000 m, with a relatively flat peak between 1000 m and 3000 m. This result is remarkably different from a single peak of the SBL. The frequency of the NBL height is generally less than 5% between 500 m and 3000 m (Fig. 5b), with a frequency peak of 6.1% at 1000 m, and more than 50% NBL height exceeds 1700 m (Fig. 5e). The height of the CBL is higher, with a frequency peak near 4.5% between 1500 m and 2500 m (Fig. 5b). More than 50% CBL height is above 2000 m (Fig. 5e). This feature is also seen at 20:00 BJT (Fig. 5c and 5f). The distributions of the NBL and CBL heights are still wide but the frequency of the high ABL height decreases, with the frequency peak below 500 m.

Because the CBL height shows a remarkable west-east difference in the TP at both 14:00 BJT and 20:00 BJT (shown in Fig. 3h-i), we analyze the cross section of the occurrence frequency of the CBL height along 32 ℃N for these two times (Fig. 6a),

https://doi.org/10.5194/acp-2020-787
Preprint. Discussion started: 24 September 2020


Atmospheric Chemistry and Physics Discussions

in which the cross section includes SQH, GZ, SZ, NQ, CD, GanZ, and HY stations. In this figure, generally speaking, the high CBL tends to occur more frequently in the WTP than in the ETP. For the ETP, the high frequency of the CBL height mainly occurs below 1400 m, with the peak of 14.4% at the height of 350 m. The occurrence frequency of the CBL height above 2000 m is low (<2%). For the WTP, there are two main peaks of the occurrence frequency. One strong peak (4%-10%) corresponds to the high CBL between 2500 m and 3500 m, especially at SQH station, and another weak peak appears between 200 m and 1000 m. The occurrence frequency is low for the CBL height between 1000 m and 2500 m. Figure 6b shows the cross section of the cumulative occurrence frequency of the CBL height along 32 ℃N. As illustrated in Fig. 6b, the cumulative frequency contours gradually go upward from east to west. The eastern TP is dominated by a low CBL height, with the 50% CBL height below 1000 m, and there is only the 5% CBL height above 2500 m. For the western TP, there are larger CBL heights, with almost 50% CBL extending upward to more than 2500 m, almost 10% reaching 4000 m or higher, and only 15% CBL below 1000 m. The above features indicate a significant difference between the ETP and the WTP in the frequency distribution of the ABL height over the TP.

To investigate an effect of differences in the sample profiles shown in Fig. 1b and d, we use the test group dataset to repeat the above analyses. Figures 7a and b show the scatter plots of the occurrence frequency of the SBL, NBL, and CBL from the original and test group datasets at each of 19 stations at 08:00 BJT and 20:00 BJT, respectively. It is seen that the correlation coefficients between the two datasets are 0.92-0.99, with root-mean-square errors (RMSEs) between 1.1% and 2.7%. The similar results are also seen in the SBL, NBL, and CBL heights at 08:00 BJT (Fig. 7c) and 20:00 BJT (Fig. 7d). The correlation coefficients in the ABL height are 0.90-0.99. The RMSE of the SBL height is 14 m and 25 m at 08:00 and 20:00 BJT, respectively. The RMSE of the CBL and NBL heights are 54-59 m at 08:00 BJT and 99-107m at 20:00 BJT. These high correlations and little errors show that the difference in the sample number does not change our conclusions.

From the foregoing analysis, the ABL height in the TP shows a remarkable diurnal variation and spatial difference, especially for both NBL and CBL. From noon to the late afternoon, there are larger NBL and CBL heights in the WTP compared to the ETP, with the differences of 668.9 m and 955.0 m between the WTP and the ETP at 20:00 BJT, respectively. Then, which factors contribute to these differences in ABL between the WTP and ETP? In the following section, we examine some factors that may be responsible for to the ABL height over the TP.

4 Factors responsible for the ABL height over the TP

A lot of studies have addressed effects of surface sensible heat flux (SHF), soil volume moisture content (VWC), downward solar radiation flux (DSR), and the total cloud cover (CLD) on ABL height (Liu, et al., 2004; Brooks and Rogers, 2006; Zhao et al., 2011; Sanchez-Mejia and Papuga, 2014; Rihani et al., 2015; Lin et al., 2016; Zhang et al., 2017; Zhang et al., 2019; Qiao et al., 2019). To investigate a possible reason for the difference in the ABL height between the eastern and

https://doi.org/10.5194/acp-2020-787
Preprint. Discussion started: 24 September 2020


Atmospheric Chemistry and Physics Discussions

western TP, we utilize the TIPEX-III SHF, DSR, VWC and CLD observations at SQH, NQ, and LZ stations, analyzing the relationships between the above variables and the ABL height.

Figure 8a-c shows the scatter plots between the 6-hour mean SHF and the ABL height at SQH, NQ, and LZ stations. As shown in this figure, the correlation is 0.80, 081, and 0.71 (significant at the 99% confidence level) at the three stations, respectively. That is, when SHF is strong, the turbulent motion is strong and the ABL height develops, which supports the result of Zhang et al. (2011b). Their result shows a significant correlation of 0.78 in the arid area of Northwest China between the ABL thickness and the cumulative SHF. Figure 9a and b further present the features of the ABL height and SHF at SQH, NQ, and LZ stations. The maximum value of SHF is 270 W/m^2, 165 W/m^2, and 100 W/m^2 at SQH, NQ and GZ stations, respectively, and has a large difference (105 W/m^2) between SQH and NQ stations. This result indicates a decreasing trend of SHF from west to east in the TP, consistent with a reduction of the ABL height from SQH via NQ to LZ station (shown in Figs. 3 and 9a). In addition, Fig. 10 demonstrates the diurnal variations of SHF and the ABL height at SQH, NQ, and LZ stations. It is clear that the peak of the SHF diurnal variation occurs earlier compared to that of the ABL height at SQH station. The maximum ABL height occurs near 20:00 BJT (approximately 17:20 LST), corresponding to a stronger SHF. At LZ station, however, the ABL height at 20:00 BJT (18:20 LST) corresponds to a negative SHF. This difference in SHF between SQH and LZ stations is possibly associated with more cloud cover (reducing the solar radiance at the surface) and one-hour time difference (an earlier transition to night at LZ station). Consequently, the difference in the ABL height between the WTP and ETP may be attributed to a west-east difference in SHF that is a direct thermal factor affecting the ABL development in the TP.

The solar radiation at the surface is an important component of the surface energy budget, affecting land surface temperature and SHF. We show the scatter plots between the 6-hour mean DSR and the ABL height at SQH, NQ, and LZ stations (Fig. 8d-f). The ABL height is highly correlated with the 6-hour average of DSR at these stations, with the correlation coefficients of 0.86, 081, and 0.73, respectively, which is equivalent to those of SHF. The mean DSR shows a decreasing trend from SQH (510 W/m^2) to LZ (200 W/m^2) station. Since the solar irradiance at the surface is negatively associated with the local cloud cover (Guo et al., 2011; Lin et al., 2016; Li et al., 2017; Zhang et al., 2017), the cloud cover is also correlated to the ABL height. Figure 8g-i show that the 6-hour mean CLD has significant correlations of -0.56, -0.65, and -0.54 with the ABL height at SQH, NQ, and LZ stations, respectively. A decrease of the mean ABL height from SQH to LZ station (Fig. 9a) is corresponded to an increase of cloud cover (Fig. 9d) and a decrease of DSR (Fig. 9c). When cloud cover is between 0 and 20%, the mean ABL height for the NBL and CBL is 2019 m /2732 m in the ETP/WTP and when cloud cover is >80%, the ABL height decreases to 741 m /1626 m in the ETP/WTP (Fig. 11). Therefore, the increased cloud cover inhibits the development of both the NBL and CBL. The difference in cloud cover between the WTP and ETP contributes to the west-east distribution of DSR and SHF, also finally contributing to the ABL development. Corresponding to more cloud cover in the ETP, the local ABL is more closely associated with atmospheric moisture processes.

https://doi.org/10.5194/acp-2020-787
Preprint. Discussion started: 24 September 2020


Atmospheric Chemistry and Physics Discussions

Soil moisture is also an important factor affecting SHF. Low soil moisture generally coincides with a high surface sensible heat flux, which facilitates the ABL development (e.g., McCumber and Pielke, 1981; Sanchez-Mejia and Papuga, 2014; Rihani et al., 2015). Figure 8j-l shows that the relationship between the ABL height and the 6-hour mean VWC at SQH, NQ, and LZ stations. The ABL height at LZ station is negatively correlated to the local soil moisture, with a significant correlation coefficient of -0.45, which indicates that the ABL height is lower when surface soil is moister. However, the negative correlation is weaker at SQH station, with a correlation coefficient of -0.21. This difference between the WTP and the ETP is associated with the climatic feature of the local soil moisture. The surface type transitions from alpine meadow with few shrubs and trees or alpine steppe in the ETP to bare soil with few obstacles in the WTP (Lin et al., 1981; Wang et al., 2016). Accordingly, soil moisture decreases gradually from the ETP to the WTP (Fig. 9e), with a mean soil moisture below 0.10 m^3/m^3 at SQH station and 0.38 m^3/m^3 at LZ station. Little soil moisture in the WTP has a weak modulation to the local surface heat flux, which results in a weak correlation between the ABL height and soil moisture in the WTP.

5 Summary and discussion

Using the summer TIPEX-III intensive and meteorological operational observational datasets, we examine the ABL features and the relationships of the ABL height with surface sensible heat flux, solar radiation, cloud cover, and soil moisture in the TP region. The main conclusions are summarized as follows.

The ABL height exhibits diurnal variations and regional differences in the TP, which are weak for SBL and remarkable for both NBL and CBL. In the early morning, the ABL height is generally low over the TP, not showing a large west-east difference, and the distribution of the ABL height is narrow, with 78.5% of the ABL height < 500 m. At noon, the CBL and NBL heights remarkably increase and have a wide distribution in the ABL height up to 4000 m, with more than 50% of the ABL height exceeding 1900 m. The height exhibits a large west-east difference. At this moment, the distribution of the SBL height is also narrow, with the cumulative frequency of 80% at the height of 500 m, and the west-east difference is not obvious. In the late afternoon, there are a narrow distribution of the SBL height and wide ones of the NBL and CBL heights. The ABL height continues to increase in the WTP, while it begins to decrease in the ETP. This feature results in a larger west-east difference in the ABL height. In spite of a cold environment in the TP (relative to plain areas), the WTP still has the ABL height above 2000 m, which is similar to some extreme hot and arid areas such as Dunhuang and Taklimakan Deserts. In the ETP, the ABL is similar to that in North China (1500-1900 m) and is generally larger compared to the East Asian summer monsoon region (＜1500 m) such as the Yangtze River Delta and the Pearl River Delta (Zhang et al., 2011; Guo et al., 2016; Zhang et al., 2017; Qiao et al., 2019).

https://doi.org/10.5194/acp-2020-787
Preprint. Discussion started: 24 September 2020


Atmospheric Chemistry and Physics Discussions

For the SBL and CBL, the occurrence frequency shows remarkable diurnal variations. Most (few) of the SBL (CBL) in the TP occur in the early morning and its occurrence frequency rapidly decreases (increases) at noon, accounting for 3.6% (76.9%) of the ABL. Moreover, possibly due to a difference in the solar elevation angle with respect to longitude in the late afternoon, the SBL and CBL dominates the ETP and WTP, respectively. However, the NBL shows a relatively weak diurnal variation over the TP, with the mean occurrence frequency of 6.4% in the early morning and around 20% at noon and in the late afternoon.

The ABL height is significantly correlated to SHF, DSR, and cloud cover in the TP and to soil moisture in the ETP. The west-east reduction in the ABL height is closely associated with the decreasing trends in both SHF and DSR and the increasing trends in both cloud cover and soil moisture from west to east. The above factors affecting the WET and ETP ABL heights are summarized in Fig. 12. That is, in the WTP (ETP), with low (high) cloud cover, there is larger (smaller) downward solar radiation at the surface. Meanwhile, corresponding to bare soil (alpine meadow or steppe) in the WTP (ETP), there is a dry (wet) soil condition. These features cause high (low) sensible heat flux, thus promoting (inhibiting) the local ABL development.

It is noted that the peak ABL height can drop from 3000–4000 m for a deep CBL in the WTP to 1000–2000 m for a shallow CBL in the ETP. Such a steep inhomogeneous distribution of the ABL height may trigger local mesoscale circulation and precipitation (Segal et al., 1992; Goutorbe et al., 1997; Huang et al., 2009; Zhang et al., 2019; Qiao et al., 2019). Therefore, the influences of west-east differences in the ABL height over the TP on the local weather and climate should be further studied in the future.

Code and data availability. All data used are available from the TIPEX-III for providing the data available on its homepages (http://data.cma.cn/tipex).

Author contributions. J.C. designed the study, analyzed the data and wrote the manuscript. P.Z. contributed to the study design and writing of the manuscript.

Competing interests. The authors declare that they have no conflict of interest.

Acknowledgements. We thank the TIPEX-III for providing the data available on its homepages (http://data.cma.cn/tipex). This work is supported by the National Key Research and Development Program of China and the Strategic Priority Research Program of Chinese Academy of Sciences.

https://doi.org/10.5194/acp-2020-787
Preprint. Discussion started: 24 September 2020


Atmospheric Chemistry and Physics Discussions

325 Financial support. This work is jointly funded by the National Key Research and Development Program of China (Grant 2018YFC1505700) and the Strategic Priority Research Program of Chinese Academy of Sciences (XDA20100300).

References

Blay-Carreras, E., Pino, D., Vil à-Guerau de Arellano, J., van de Boer, A., De Coster, O., Darbieu, C., Hartogensis, O., Lohou, F., Lothon, M., Pietersen, H.: Role of the residual layer and large-scale subsidence on the development and evolution of the 330 convective boundary layer, Atmos. Chem. Phys., 14, 4515-4530, doi: 10.5194/acp-14-4515-2014, 2014.

Brooks, I. M., Rogers, D. P.: Aircraft observations of the mean and turbulent structure of a shallow boundary layer over the Persian Gulf, Boundary-Layer. Meteorology, 95, 189-210, doi:10.1023/A:1002623712237, 2000.

Chen, S. S., and Houze, R. A.: Diurnal variation and life-cycle of deep convective systems over the tropical Pacific warm pool, Quart. J. Roy. Meteor. Soc., 123, 357–388, doi: 10. 1002/qj.49712353806, 1997.

335 Chen, X. L., Juan, A. Añel., Su, Z. B., Laura, de. La. Torre., Hennie, Kelder., Jacob, van. Peet., Ma, Y. M.: The deep atmospheric boundary layer and its significance to the stratosphere and troposphere exchange over the Tibetan Plateau, PLoS. ONE, 8, e56909, doi: 10.1371/journal.pone.0056909, 2013.

Chen, X. L., Škerlak, B., Rotach, M. W., Juan, A. Anel., Su, Z. B., Ma, Y. M., Li, M. S.: Reasons for the extremely high-ranging planetary boundary layer over the Western Tibetan Plateau in winter, J. Atmos. Sci, 73, 2021-2038, doi: 10.1175/jas-340 d-15-0148.1, 2016.

Dai, C., Wang, Q., Kalogiros, J. A., Lenschow, D. H., Gao, Z., Zhou, M.: Determining Boundary-Layer Height from Aircraft Measurements, Bound.-Lay. Meteorol., 152, 277–302, doi:10.1007/s10546-014-9929-z, 2014.

Davy, R.: The climatology of the atmospheric boundary layer in contemporary global climate models. Journal of Climate, doi: 10.1175/JCLI-D-17-0498.1, 2018.

345 Garratt, J. R.: The Atmospheric Boundary Layer, Cambridge, Univ. Press., 37, 89-134, doi: 10.1007/3-211-38078-7_4, 1992.

Goutorbe, J. P., Lebel, T., Dolman, A. J., Gash, J. H. C., Kabat, P., Kerr, Y. H., Monteny, B., Prince, S. D., Stricker, J. N. M., Tinga, A., Wallace, J. S.: An overiew of HAPEX-Sahel: A study in climate and desertification, Journal. of Hydrol., 188-189, 4-17, doi:10.1016/S0022-1694(96) 03308-2, 1997.

Guo, J. P., Zhang, X. Y., Che, H. Z., Gong, S. L., An, X., Cao, C. X.: Correlation between PM concentrations and aerosol 350 optical depth in eastern China, Atmos. Environ., 43, 5876-5886, doi: 10.1016/j.atmosenv.2009.08. 026, 2009.

Guo, J. P., Miao, Y. C., Zhang, Y., Liu, H., Li, Z. Q., Zhang, W. C., He, J., Lou, M. Y., Yan, Y., Bian, L. G., Zhai, P. M.: The climatology of planetary boundary layer height in China derived from radiosonde and reanalysis data, Atmospheric. Chemistry. and Physics., 16, 13309-13319, doi:10.5194/acp-16-13309-2016, 2016.

Hong, J., Guo, J., Du, J., Wang, P.: An observational study on the vertical structure of the upper troposphere and lower 355 stratosphere in Gaize, Tibet during the rainy season, Acta. Meteor. Sin., 74, 827-836, doi:10.11676/qxxb2016.05, 2016.

Huang, J. P., Minnis, P., Yi, Y., Tang, Q., Wang, X., Hu, Y., Liu, Z., Ayers, K., Trepte, C., Winker, D.: Summer dust aerosols detected from CALIPSO over the Tibetan Plateau, Geophys. Res. Lett., 34, L18805, doi:10.1029/2007GL029938, 2007.

Huang, Q., Marsham, J. H., Parker, D. J., Tian, W., Weckwerth, T.: A comparision of roll and nonroll convection and the subsequent deepening moist convection: An LEM case study based on SCMS data, Mon. Wea. Rev., 137, 350-365, doi:10.1175/2008MWR2450.1, 2009.

Li, J. L., Hong, Z. X., Sun, S. F.: An observational experiment on the atmospheric boundary layer in Gerze area of the Tibetan Plateau, Chinese. J. Atmos. Sci., 24, 301-312, doi: 10.3878/j.issn.1006-9895.2000.03.02, 2000.

Li, Y., Gao, W.: Atmospheric boundary layer circulation on the eastern edge of the Tibetan Plateau, China, in summer, Arct. Antarct. Alp. Res., 39, 708-713, doi: 10.1657/1523-0430(07-50 4)[li]2.0.co;2, 2007.

Li, M. S., Ma, Y. M., Ma, W. Q., Ishikawa, Hirohiko., Sun, F. L., Ogino, S. Y.: Structural difference of atmospheric boundary layer between dry and rainy seasons over the central Tibetan Plateau, Journal. of Glaciology. and Geocryology., 33, 72-79, doi:10.3724/SP.J.1146.2006.01085, 2011.

Li, Z., Guo, J., Ding, A., Liao, H., Liu, J., Sun, Y.: Aerosol and boundary-layer interactions and impact on air quality, Natl. Sci. Rev., 4, 810-833, doi:10.1093/nsr/nwx117, 2017.

Li, N., Zhao, P., Wang, J., Deng, Y.: Estimation of surface heat fluxes over the central Tibetan Plateau using the maximum entropy production model. Journal of Geophysical Research: Atmospheres, 124, 6827–6840, doi:10.1029/2018JD029959, 2019.

Li, N., Zhao, P., Wang, J., Deng, Y.: The Long-Term Change of Latent Heat Flux over the Western Tibetan Plateau. Atmosphere, 11, 262, doi: 10.3390/atmos11030262, 2020.

Lin, Y., Wang, Y., Zhang, R., Liu, Y.: Response of boundary layer clouds to continental pollution during the RACORO campaign, J. Atmos. Sci., 73, 3681–3700, doi: 10.1175/JAS-D-15-036 1.1, 2016.

Liu, S. H., Xu, Y., Hu, F.: Using a Modified Soil-Plant-Atmosphere Scheme (MSPAS) to simulate the interaction between land surface processes and atmospheric boundary layer in semi-arid regions. Advances in Atmospheric Sciences, 21(2): 245-259, doi: 10.1007/bf029157 11, 2004.

Liu, S. Y., Liang, X. Z.: Observed diurnal cycle climatology of planetary boundary layer height, Journal. of Climate., 23, 5790-5809, doi:10.1175/2010JCLI3552.1, 2010.

Liu, H. Y., Miao, M. Q.: Preliminary analysis on characteristics of boundary layer in Qinghai-Tibet Plateau, Journal. of Nanjing. University. (Natural. Sciences.)., 37, 348-357, doi: 10.3321/j.issn:0469-5097.2001.03.013, 2001.

Lü, Y. Q., Ma, Y. M., Li, M. S., Sun, F. L.: Study on characteristic of atmospheric boundary layer over Lake Namco region, Tibetan Plateau, Plateau. Meteorology., 27, 1205-1210, doi: ir.casnw.net/handle/362004/9294, 2008.

McCumber, M. C., and Pielke, R. A.: Simulation of the effects of surface fluxes of heat and moisture in a mesoscale numerical model: 1. Soil layer, J. Geophys. Res., 86, 9929-9938, doi:10.1029/JC086iC10p09929, 1981.

https://doi.org/10.5194/acp-2020-787
Preprint. Discussion started: 24 September 2020


Atmospheric Chemistry and Physics Discussions

Miao, Y. C., Hu, X. M., Liu, S. H., Qian, T. T., Xue, M., Zheng, Y. J., Wang, S.: Seasonal variation of local atmospheric circulations and boundary layer structure in the Beijing-Tianjin-Hebei region and implications for air quality, Journal. of Advances. in Modeling. Earth. Systems., 7, 1602-1626, doi: 10.1002/2015MS000 522, 2015.

Pal, S., and Haeffelin, M.: Forcing mechanisms governing diurnal, seasonal, and interannual variability in the boundary layer depths: Five years of continuous lidar observations over a suburban site near Paris, J. Geophys. Res. Atmos., 120, 11936-11956, doi: 10.1002/2015JD023268, 2015.

Qiao, L., Zhang, Q., Yue, P., et al.: Analysis of changes in the structure of atmospheric boundary layer from non-monsoon zone to monsoon zone, Chinese Journal of Atmospheric Sciences, 43 (2): 251-265, doi: 10.3878/j.issn.1006-9895.1 805.17231, 2019.

Raman, S., Templeman, B., Templeman, S., Holt, T., Murthy, A. B., Singh, M. P., Agarwaal, P., Nigam, S., Prabhu, A., Ameenullah, S.: Structure of the Indian southwesterly pre-monsoon and monsoon boundary layers: Observations and numerical simulation, Atmos. Environ., 24, 723-734, doi: 10.1016/0960-1686(90)90273-p, 1990.

Rihani, J. F., Chow, F. K., Maxwell, R. M.: Isolating effects of terrain and soil moisture heterogeneity on the atmospheric boundary layer: Idealized simulations to diagnose land atmosphere feedbacks, J. Adv. Model. Earth Syst., 7, 915-937, doi: 10.1 002/2014MS000371, 2015.

Sanchez-Mejia, Z. M., and Papug, S. A.: Observations of a two-layer soil moisture influence on surface energy dynamics and planetary boundary layer characteristics in a semiarid shrubland, Water. Resour. Res., 50, 306-317, doi:10.1002/2013WR014135, 2014.

Segal, M., Arritt, R. W.: Nonclassical mesoscale circulations caused by surface sensible heat-flux gradients, Bull. Amer. Meteor. Soc., 73, 1593-1604, doi:10.1175/1520-0477(1992) 0732.0.CO;2, 1992.

Seibert, P., Beyrich, F., Gryning, S. E., Joffre, S., Rasmussen, A., Tercier, P.: Review and intercomparison of operational methods for the determination of the mixing height, Atmos. Environ., 34, 1001-1027, doi: 10.1016/s1352-2310(99)00349-0, 2000.

Seidel, D. J., Ao, C. O., Li, K.: Estimating climatological planetary boundary layer heights from radiosonde observations: Comparison of methods and uncertainty analysis, Journal. of Geophysical. Research. Atmospheres., 115, D16113, doi:10.1016/s1352-2310(99)00349-0, 2010.

Seidel, D. J., Zhang, Y., Beljaars, A., Golaz, J.-C., Jacobson, A. R., Medeiros, B.: Climatology of the planetary boundary layer over the continental United States and Europe, Journal. of Geophysical. Research.: Atmospheres., 117, D17106, doi: 10.1029/2012jd018143, 2012.

Stull, R. B.: An Introduction to Boundary Layer Meteorology, Springer. Netherlands., doi:10.1007/978-94-009 -3027-8, 1988.

Sun, F., Ma, Y., Li, M.: Boundary layer effects abovea Himalayan valley near Mount Everest, Geophys. Res. Lett., 34, L08808, doi: 10.1029/2007gl029484, 2007.

Tao, S. Y., Ding, Y. H.: Observational evidence of the influence of the Qinghai-Xizang (Tibet) Plateau on the occurrence of heavy rain and severe convective storms in China, Bulletin. of the American. Meteorological. Society., 62, 23-30, doi:10.1175/1520-0477(1981)062h0023:OEOTIOi2.0.CO;2, 1981.

Wang, Y. J., Xu, X. D., Liu, H. Z., Li, Y. Q., Li, Y. H., Hu, Z. Y., Gao, X. Q., Ma, Y. M., Sun, J. H., Lenschow, D. H., Zhong, S. Y., Zhou, M. Y., Bian, X. D., Zhao, P., Wang, Y. J.: Analysis of land surface parameters and turbulence characteristics over the Tibetan Plateau and surrounding region, J. Geophys. Res. Atmos., 121, 9540-9560, doi:10.1002/2016JD025401, 2016.

Xu, X., Bian, L., Zhang, G., Bian, L. G., Zhang, G. Z., Liu, H. Z.: A comprehensive physical pattern of land-air dynamic and thermal structure on the Qinghai-Xizang Plateau, Science. in China. Series. D.: Earth. Sciences., 45, 577-594, doi:10.1360/02yd9060, 2002.

Yanai, M., Li, C.: Mechanism of heating and the boundary layer over the Tibetan Plateau, Mon. Wea. Rev., 122, 305-323, doi:10.1175/1520-0493(1994)1222.0.CO;2, 1994.

Yang, K., Koike, T., Fujii, H., Tamura, T., Xu, X., Bian, L., Zhou, M. Y.: The daytime evolution of the atmospheric boundary layer and convection over the tibetan plateau: observations and simulations (regional climate modeling for monsoon system), Journal. of the Meteorological. Society. of Japan., 82, 1777-1792, doi:10.2151/jmsj.82.1777, 2004.

Ye, D., Gao, Y. X.: The Meteorology of the Qinghai-Xizang Plateau, Beijing.: Science. Press., 89-101, 1979.

Yu, X. J., Du, J., Wang, M. Z., Xu, H. X., He, Q.: Impact of assimilating the new radiosonde data on qinghai-tibetan plateau on summer rainfall forecast over southern xinjiang, Plateau. Meteorology., 2018.

Zhang, G., Xu, X., Wang, J.: A dynamic study of Ekman characteristics by using 1998 SCSMEX and TIPEX boundary layer data, Advances. in Atmospheric. Sciences., 20, 349-356, doi: 10.1007/bf02690793, 2003.

Zhang, Y., Seidel, D. J., Golaz, J.-C., Deser, C., Tomas, R. A.: Climatological characteristics of Arctic and Antarctic surface-based inversions, J. Climate., 24, 5167-5186, doi: 10.1 175 /2011JCLI4004.1, 2011a.

Zhang, Q., Zhang, J., Qiao, J., Wang, S.: Relationship of atmospheric boundary layer depth with thermodynamic processes at the land surface in arid regions of China, Sci. China: Earth. Sci., 54, 1586-1594, doi:10.1007/s11430-011-4207-0, 2011b.

Zhang, Q., Yue, P., Zhang, L., et al.: Land-atmosphere interaction over the summer monsoon transition zone in China: A review and prospects, Acta. Meteorologica. Sinica., 77, 758-773, 2019.

Zhang, W., Guo, J., Miao, Y., Liu, H., Yang, S., Fang, Z., He, J., Lou, M. Y., Yan, Y., Li, Y., Zhai, P. M.: On the summertime planetary boundary layer with different thermodynamic stability in China: a radiosonde perspective, Journal, of Climate., 31, doi: 10.1175/jcli-d-17-0231.1, 2017.

Zhao, C. L.， Li, Y. H., Liu, Y. P., et al.: The variation characteristics of planetary boundary layer height in Northwest China: Based on radiosonde and ERA-Interim reanalysis data, Plateau. Meteorology., 38, 1181-1193, doi: 10.7522 /jissn.1000－0534.2018.00152, 2019a.

Zhao, J. H., Zhang, Q., Wang, S.: A simulative study of the thermal mechanism for development of the convective boundary layer in the arid zone of Northwest China, Acta. Meteorologica. Sinica., 69, 1029-1037, doi:10.11676/qxxb2011.090, 2011.

https://doi.org/10.5194/acp-2020-787
Preprint. Discussion started: 24 September 2020

Atmospheric Chemistry and Physics Discussions

Zhao, M., Miao, M. Q.: The atmospheric boundary layer, Beijing: China. Meteorological. Press., 1992.

Zhao, P., Xu, X., Chen, F., et al.: The Third Atmospheric Scientific Experiment for understanding the earth–atmosphere coupled system over the Tibetan Plateau and its effects, Bull. Amer. Meteor. Soc., 99, 757-776, doi: 10.1175/BAMS-D-16-0050.1, 2018.

Zhao, P., Li, Y. Q., Guo, X. L., et al.: The Tibetan Plateau surface-atmosphere coupling system and its weather and climate effects: The Third Tibetan Plateau Atmospheric Science Experiment, J. Meteor. Res., 33, 375-399, doi: 10.1007/s13351-019-8602-3, 2019b.

Zhou, W., Yang, S. P., Jiang, X., et al: Estimating palnetary boundary layer height over the Tibetan Plateau using COSMIC radio occultation data, Acta. Meteorologica. Sinica., 76, 117-133, doi: 10.11676/qxxb2017.069, 2018.

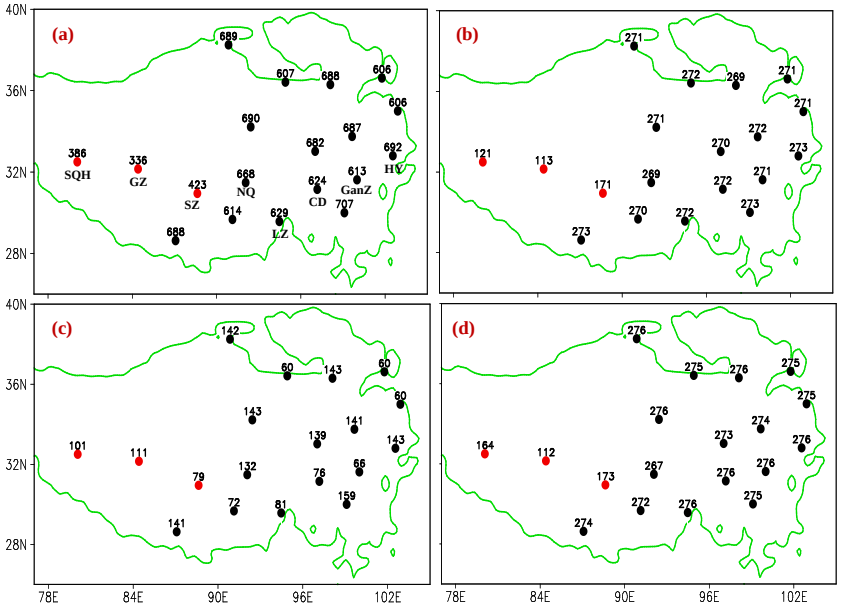

Figure 1: Distribution of sounding stations, in which the number indicates sounding profiles at each station at (a) all times, (b) 08:00 BJT, (c) 14:00 BJT, and (d) 20:00 BJT in the study period. Red (black) dots represent intensive (operational) sites. Some letters are for the abbreviated names of stations. The green line is for the topography above 3 km.

https://doi.org/10.5194/acp-2020-787
Preprint. Discussion started: 24 September 2020

Atmospheric Chemistry and Physics Discussions

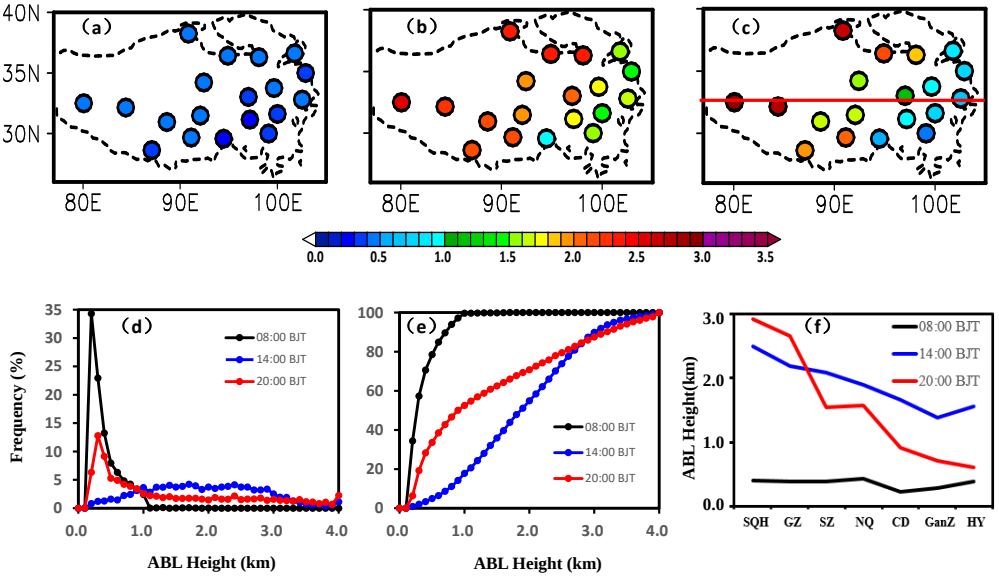

Figure 2: Spatial distribution of the mean ABL height for all types at (a) 00:08 BJT, (b) 14:00 BJT, and (c) 20:00 BJT in the study period; (d) the regional mean frequency and (e) cumulative frequency distributions of the ABL height over the TP at 08:00 BJT, 14:00 BJT, and 20:00 BJT; (f) the west-east cross section of the ABL height along 32 ℃N (red line shown in (c)) at 08:00 BJT, 14:00 BJT, and 20:00 BJT.

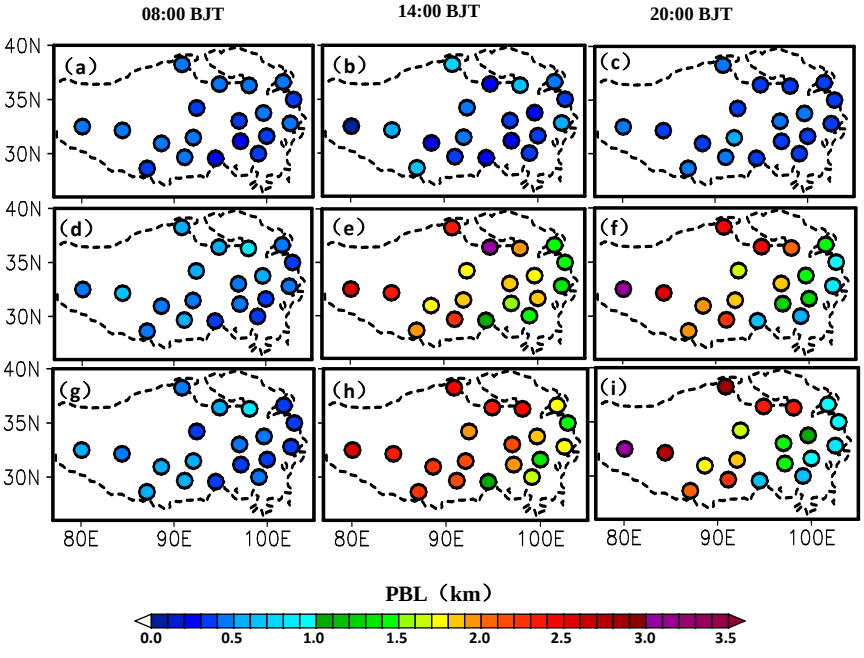

Figure 3: Same as in Fig. 2a but for the SBL (top), NBL (middle), and CBL (bottom) at 08:00 BJT, 14:00 BJT, and 20:00 BJT.

https://doi.org/10.5194/acp-2020-787
Preprint. Discussion started: 24 September 2020

Atmospheric Chemistry and Physics Discussions

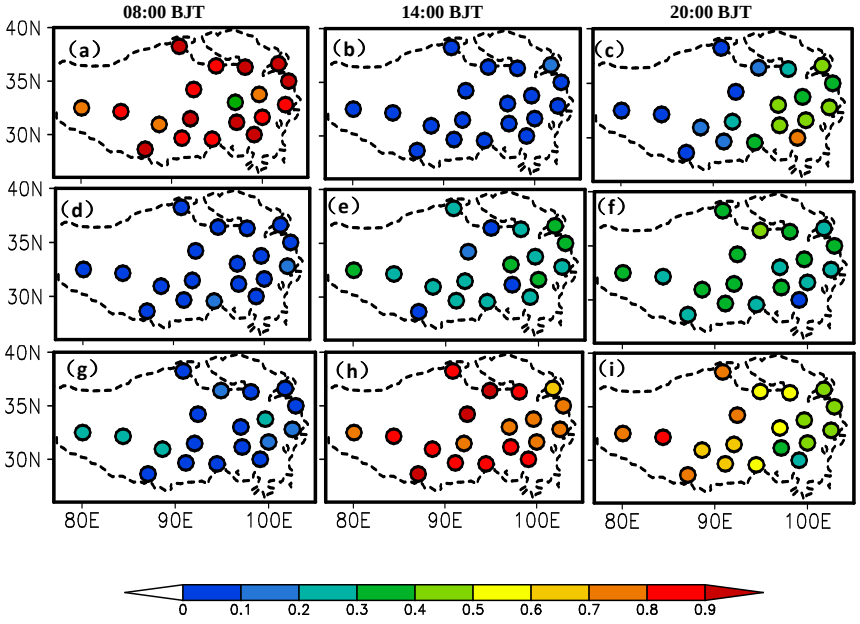

480 **Figure 4: Same as in Fig. 3 but for the occurrence frequency.**

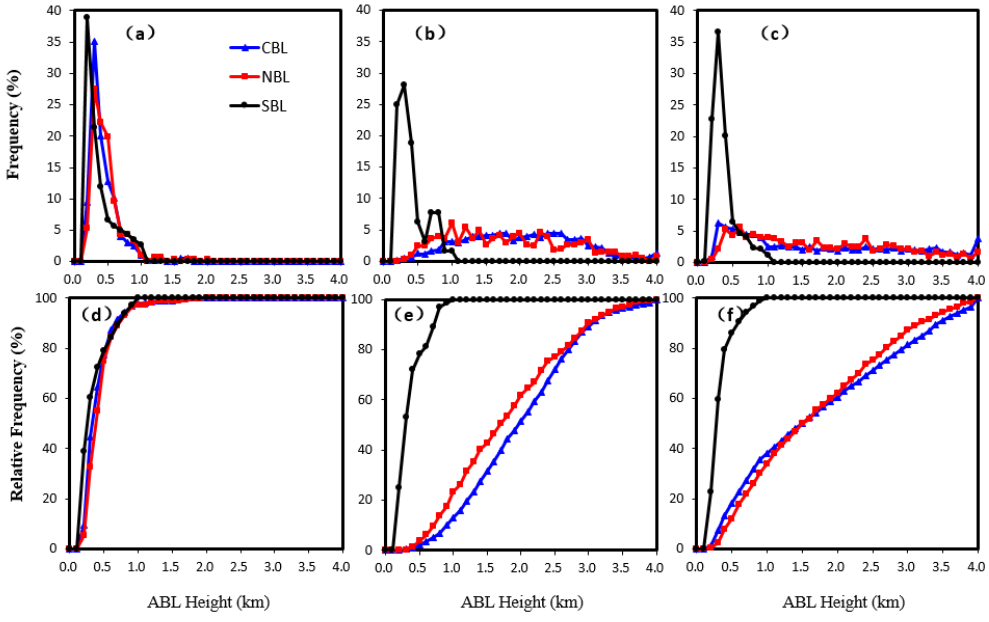

Figure 5: The regional mean frequency distributions of the ABL height over the TP for the CBL (blue), NBL (red), and SBL (black) in the study period at (a) 08:00 BJT, (b) 14:00 BJT, and (c) 20:00 BJT; and (d)-(f) same as in (a)-(c) but for the cumulative frequency distributions.

https://doi.org/10.5194/acp-2020-787
Preprint. Discussion started: 24 September 2020

Atmospheric Chemistry and Physics Discussions

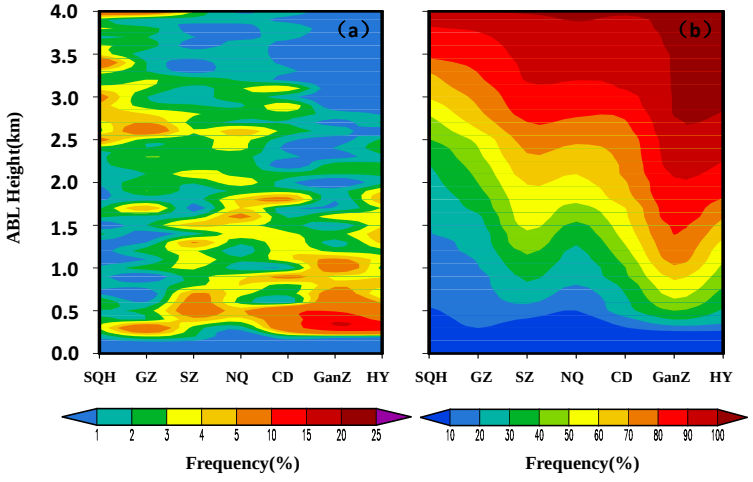

Figure 6: The west-east cross section of frequency (a) and cumulative frequency (b) distributions of the CBL height along 32 ℃N in daytime (14:00 and 20:00 BJT).

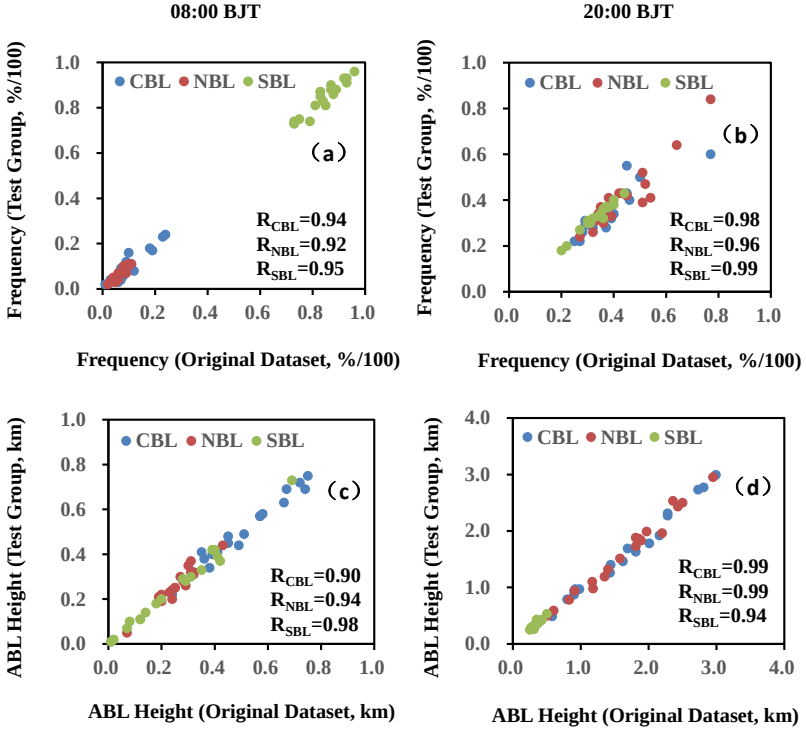

Figure 7: The scatter plots of the occurrence frequency of the SBL, NBL, and CBL from the original and test group datasets at each of 19 stations at (a) 08:00 BJT and (b) 20:00 BJT; and (c)-(d) same as in (a)-(b) but for the ABL height.

https://doi.org/10.5194/acp-2020-787
Preprint. Discussion started: 24 September 2020

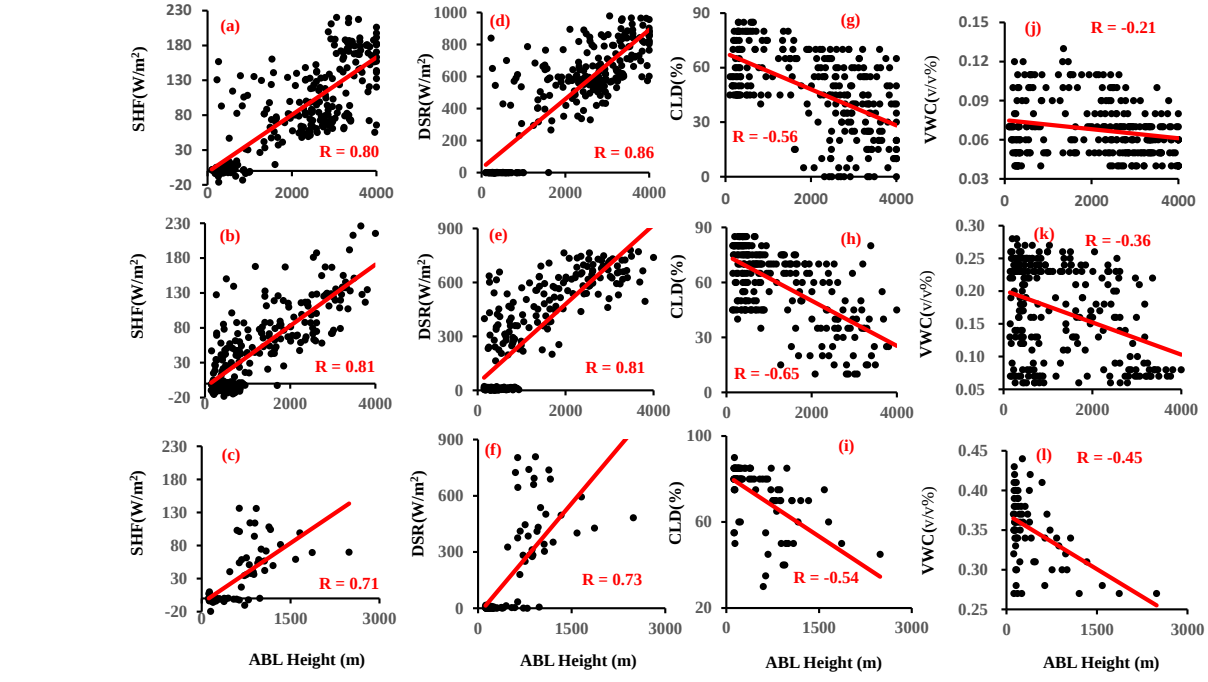

Figure 8: Scatter plots of the ABL height and the 6-hour average of surface sensible heat flux (SHF) (a-c), surface downward solar radiation flux (DSR) (d-f), total cloud coverage (CLD) (g-i), and surface soil volume moisture content (VWC) (j-l) at 08:00 BJT, 14:00 BJT, and 20:00BJT at SQH (top), NQ (middle), and LZ (bottom) stations in the study period. The correlation coefficient (R) is given in each panel.

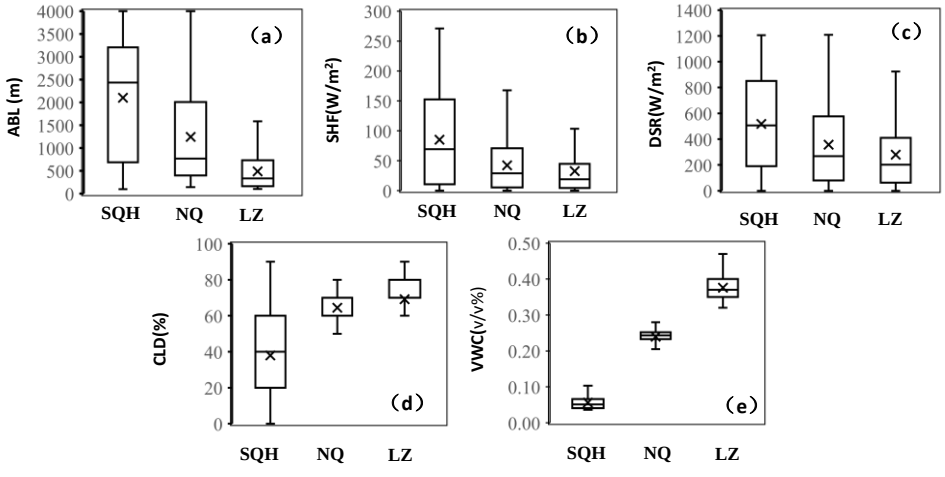

Figure 9: (a) The ABL height, (b) SHF, (c) DSR, (d) CLD, and (e) VWC at SQH, NQ, and LZ stations in the study period. Horizontal bars show the 5th, 25th, 50th, 75th, and 95th percentile values and "×" symbols show the corresponding mean value.

https://doi.org/10.5194/acp-2020-787
Preprint. Discussion started: 24 September 2020

Atmospheric Chemistry and Physics Discussions

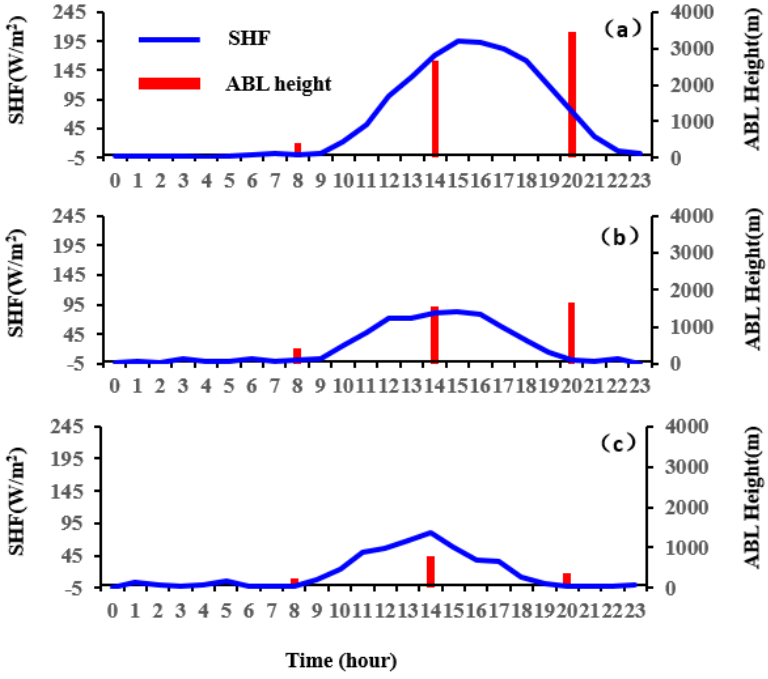

Figure 10: Diurnal variations of surface sensible heat flux (blue) and the ABL height (red) at (a) SQH, (b) NQ, and (c) LZ stations averaged over the study period.

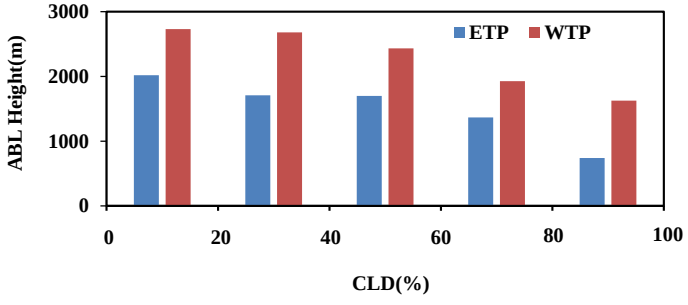

Figure 11: The mean ABL height (for the NBL and CBL) and CLD over the ETP (blue) and WTP (red) in daytime (14:00 BJT and 20:00 BJT).

https://doi.org/10.5194/acp-2020-787
Preprint. Discussion started: 24 September 2020

Atmospheric Chemistry and Physics Discussions

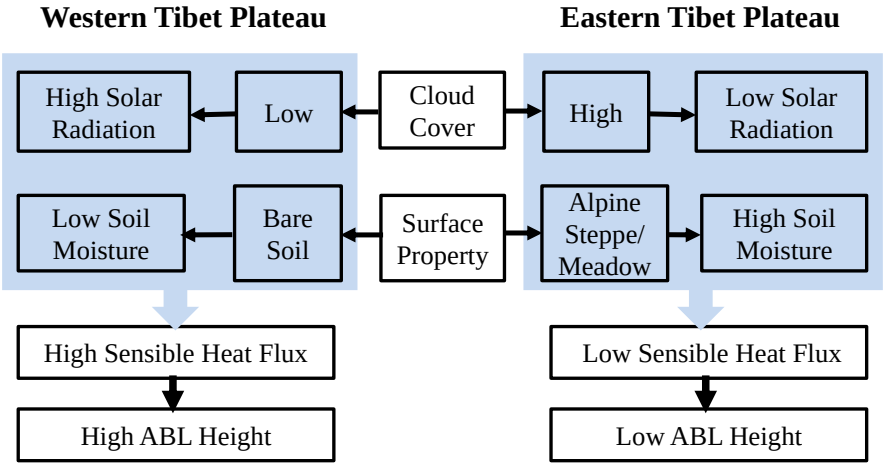

505

Figure 12: A schematic diagram for relationships between the ABL height and the influential factors in the ETP and the WTP.